A Grid-Tied AC Drive Using a Multilevel Topology Obtained from the Nine-Switch Converter

Joaquim Monteiro
UnIRE, ISEL, Polytechnic University of Lisbon, Portugal
INESC-ID Lisboa, Portugal
joaquim.monteiro@isel.pt

V. Fernão Pires
ESTSetúbal, Instituto Politécnico Setúbal, Setubal, Portugal
INESC-ID Lisboa, Portugal
vitor.pires@estsetubal.ips.pt

J. Fernando Silva
DEEC, IST, Universidade de Lisboa, Lisboa, Portugal
INESC-ID Lisboa, Portugal
fernando.alves@tecnico.ulisboa.pt

Sónia Pinto
DEEC, IST, Universidade de Lisboa, Lisboa, Portugal
INESC-ID Lisboa, Portugal
soniafp@tecnico.ulisboa.pt

***Abstract* – Nine-switch inverters, has been widely used in several power systems applications, especially for a dual motor or six-phase machine. Due to their interesting features such as the reduced switch number, this structure has been extended to multilevel topologies. Among the several multilevel topologies, the active-neutral-point-clamped (ANPC) based nine-switch multilevel converter (ANPC-NSMC) has been one of the interesting solutions. In this paper, instead of using this topology for a dual motor or six-phase motor, it is proposed a back-to-back application. In this way, one of the outputs is connected to the grid, while the other output is connected to the three-phase motor. However, for drives a closed loop control is needed. Therefore, a field-oriented controller and a model predictive control (MPC) strategy to control this AC drive is also proposed. The MPC will be used for closed loop current control, as well as for mitigation of the capacitor voltages imbalance. This optimal predictive controller allows the minimization of a cost functional weighing three criteria, the tracking errors of the three-phase AC currents of each side, as well as the two capacitors voltage imbalance. The performance of the proposed control strategy will be verified and discussed through several simulations results.**

Keywords – AC motor drive; Dual output inverter, nine-switch multilevel coverter, NPC-Type converter; model predictive control.

I. INTRODUCTION

Over the last few decades, the development of power converter topologies has mainly focused on reducing the switching voltage distortion, thereby improving the power quality at the converter output. The multilevel converter is an example of these enhancements. This converter has many advantages when compared to the conventional two-level topologies, particularly regarding the power quality of the output voltages and the reduction of harmonic content [1]. Due to these characteristics, the multilevel converter has been extended to many applications, namely energy storage systems, renewable energy sources, power transmissions systems, electrical drives, among other applications [2,3].

The most commonly used multilevel converter topologies in AC motor drives are the Neutral Point Clamped (NPC), Flying Capacitor (FC), and Cascaded H-Bridge Inverter (CHB) [4-6]. In addition to these classic topologies, numerous variants have emerged that are advantageous for certain applications [7-12]. These multilevel converters were initially used for medium voltage AC drives, but they were quickly extended to low voltage AC drives. Several multilevel topologies have been proposed for use in AC motor drives, with the primary goal of reducing the volume and cost of drive converters, by reducing the semiconductor count. An example of these topologies is the Packed U Cells (PUC) [13].

For AC grid powered drives, among the various proposed multilevel structures, those with dual output can interconnect the drive to the AC grid. This converter presents an active-neutral-point-clamped (ANPC) type structure based on the nine-switch inverter [14]. The ANPC based nine-switch multilevel converter (ANPC-NSMC) has a smaller number of components (diodes and switches) comparatively to the equivalent two ANPC multilevel conventional inverters, allowing high performance and reduced switching losses [15]. Industrial applications of the ANPC-NSMC have already been disclosed in numerous works, revealing the wide range of the ANPC-NSMC utilization. The most valuable attribute is the capability to ensure dual voltage output, ideal for several applications, specifically those involving dual motor drives [16]. The nine-switch converter topology is also commonly used in back-to-back structures, both in reactive power compensation using induction motor [17], or applied to energy power generation systems, using for a squirrel cage induction generator [18]. However, in these solutions a classic two-level topologies converters were used.

The control of the ANPC-NSMC was subject of several research works in closed-loop control, operating under nominal operating conditions. However, many of these works are based on pulse-width modulation (PWM) techniques [17], [19]. In [19] an inverter with dual outputs with a modulation strategy that incorporates both time-sharing modulation and virtual space vector pulse-width modulation (VSVPWM) was presented. Nevertheless, these modulation techniques exhibit issues to the control of the AC currents, in both outputs, as well as in the balance of the voltages in the DC capacitors. These restraints can be solved by applying techniques, based on predictive control, widely used in power electronic [20-22]. In [23], a controller for the three-phase dual output multilevel converter based on the model predictive control (MPC) was proposed. Indeed, the MPC has several interesting features, including a simple concept, fast dynamic responses, and readiness for multivariable systems [24].
The nine-switch inverter is typically used in dual or six-phase drives. However, in this paper, it is proposed to use the ANPC-NSMC topology for a back-to-back solution, in which one of the outputs is connected to the grid while the other is connected to an induction motor. Regarding its closed loop control, among the various control techniques used in AC motor drives a field-oriented controller and an MPC strategy to control this AC drive is hereafter presented. The MPC will be used for closed-loop current control, as well as for mitigation of the capacitor imbalance voltages. This controller allows the minimization of a cost functional weighing three criteria, the tracking errors of the three-phase AC currents, on both sides, and the capacitor imbalance voltages of the ANPC-NSMC. The proposed power system will be tested through a case study by using a numerical program. From the results obtained both in a stationary and transient state, it is concluded the obtained AC drive presents

2024 IEEE 18th International Conference on Compatibility, Power Electronics and Power Engineering (CPE-POWERENG) | 979-8-3503-1826-5/24/$31.00 ©2024 IEEE | DOI: 10.1109/CPE-POWERENG60842.2024.10604329

high dynamic performance, validating the theoretical analysis of the proposed solution.

II. Model of the Nine-Switch Multilevel Converter

The ANPC-NSMC topology based on a three-level ANPC-type inverter is presented in Fig. 1. This multilevel structure allows a dual port three-level inverter, by using the common switches in the same way as the 9-switch inverter, reducing volume and cost [15]. The ANPC-NSMC upper interface, identified as the rectifier, connects to the grid through an impedance *Rg* and *Lg*. On the other hand, the ANPC-NSMC lower interface, identified as the inverter, connects to an induction motor (IM).

The nine-switch converter can be modeled considering that the power semiconductors are represented by ideal switches. The active switch state can be represented by a binary variable, defined as follows:

$$\begin{cases} \gamma_{ij} = 1 \quad , \quad if\ S_{ij}\ is\ ON \\ \gamma_{ij} = 0 \quad , \quad if\ S_{ij}\ is\ OFF \end{cases}, \quad \text{with } i{=}A,B,C \text{ and } j{=}1..7 \tag{1}$$

From the power circuit analysis, the voltages between the upper and lower AC terminals of the ANPC-NSMC and the middle point of the capacitors can also be defined as functions of the switches states (2).

$$\begin{cases} v_{Ui0} = \dfrac{V_{DC}}{2}\left(\gamma_{i1}\gamma_{i2} - \gamma_{i3}\gamma_{i4}\gamma_{i5}\right)\left(1-\gamma_{i2}\gamma_{i6}\right) \\ v_{Li0} = \dfrac{V_{DC}}{2}\left(\gamma_{i1}\gamma_{i2}\gamma_{i3} - \gamma_{i4}\gamma_{i5}\right)\left(1-\gamma_{i4}\gamma_{i7}\right) \end{cases} \tag{2}$$

According to the previous mathematical relationships, the following switching functions will be defined:

$$\begin{cases} \alpha_{Ui} = \dfrac{1}{2}\left(\gamma_{i1}\gamma_{i2} - \gamma_{i3}\gamma_{i4}\gamma_{i5}\right)\left(1-\gamma_{i2}\gamma_{i6}\right) \\ \alpha_{Li} = \dfrac{1}{2}\left(\gamma_{i1}\gamma_{i2}\gamma_{i3} - \gamma_{i4}\gamma_{i5}\right)\left(1-\gamma_{i4}\gamma_{i7}\right) \end{cases} \tag{3}$$

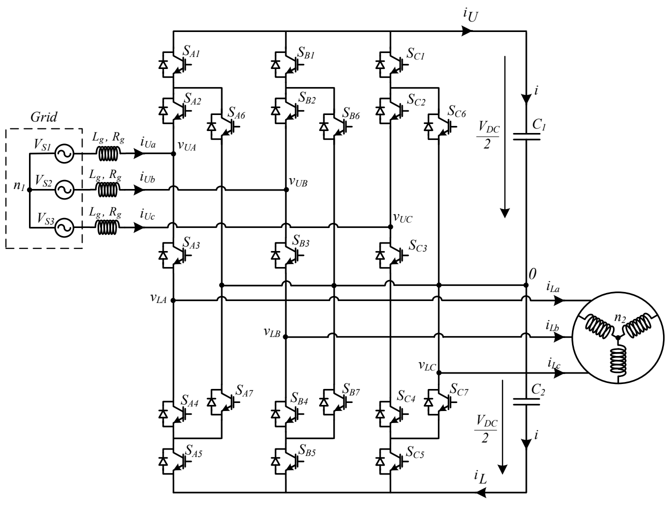

Fig. 1. Power circuit of the ANPC-NSMC connected to the IM and to the grid.

The previous expressions allow the formulation of the mathematical model for the voltages applied to the load, in (4) and to the grid in (5).

$$\begin{bmatrix} v_{UAn1} \\ v_{UBn1} \\ v_{UCn1} \end{bmatrix} = \frac{V_{DC}}{3} \begin{bmatrix} 2 & -1 & -1 \\ -1 & 2 & -1 \\ -1 & -1 & 2 \end{bmatrix} \begin{bmatrix} \alpha_{UA} \\ \alpha_{UB} \\ \alpha_{UC} \end{bmatrix} \tag{4}$$

$$\begin{bmatrix} v_{LAn2} \\ v_{LBn2} \\ v_{LCn2} \end{bmatrix} = \frac{V_{DC}}{3} \begin{bmatrix} 2 & -1 & -1 \\ -1 & 2 & -1 \\ -1 & -1 & 2 \end{bmatrix} \begin{bmatrix} \alpha_{LA} \\ \alpha_{LB} \\ \alpha_{LC} \end{bmatrix} \tag{5}$$

Converting the previous three-phase voltages in two phase orthogonal system through the application of the Clark-Concordia transformation, equation (6) and (7) are obtained, respectively for the load and for the grid.

$$\begin{bmatrix} v_{U\alpha} \\ v_{U\beta} \end{bmatrix} = V_{DC} \begin{bmatrix} \sqrt{\frac{2}{3}} & -\frac{1}{\sqrt{6}} & -\frac{1}{\sqrt{6}} \\ 0 & \frac{1}{\sqrt{2}} & -\frac{1}{\sqrt{2}} \\ -1 & -1 & 2 \end{bmatrix} \begin{bmatrix} \alpha_{UA} \\ \alpha_{UB} \\ \alpha_{UC} \end{bmatrix} \tag{6}$$

$$\begin{bmatrix} v_{L\alpha} \\ v_{L\beta} \end{bmatrix} = V_{DC} \begin{bmatrix} \sqrt{\frac{2}{3}} & -\frac{1}{\sqrt{6}} & -\frac{1}{\sqrt{6}} \\ 0 & \frac{1}{\sqrt{2}} & -\frac{1}{\sqrt{2}} \\ -1 & -1 & 2 \end{bmatrix} \begin{bmatrix} \alpha_{LA} \\ \alpha_{LB} \\ \alpha_{LC} \end{bmatrix} \tag{7}$$

By analysing equations (6) and (7) and considering the combination of all the states γ_{ij} of the power semiconductors, 216 different output voltage space vectors are obtained. Several of these vectors are redundant from the standpoint of AC voltages, but not for the DC capacitor voltages.

III. Control of the Nine-Switch Multilevel Converter

The control system employed in this NSMC fed induction motor drive is based on the field-oriented controller (FOC) and on the predictive control. This vector control method, widely used to control AC synchronous and induction motors, generates the stator current references, to apply to the MPC, on the inverter side. On the other hand, the reference values for the grid currents predictive controller are obtained from the DC-link voltage error through a Proportional Integral (PI) controller that keeps the DC-link voltage nearly constant, according to the scheme of Fig.2 [21]. Afterwards, this controller determines the optimal switching state, out of the available 216, to be applied during the next sample period.

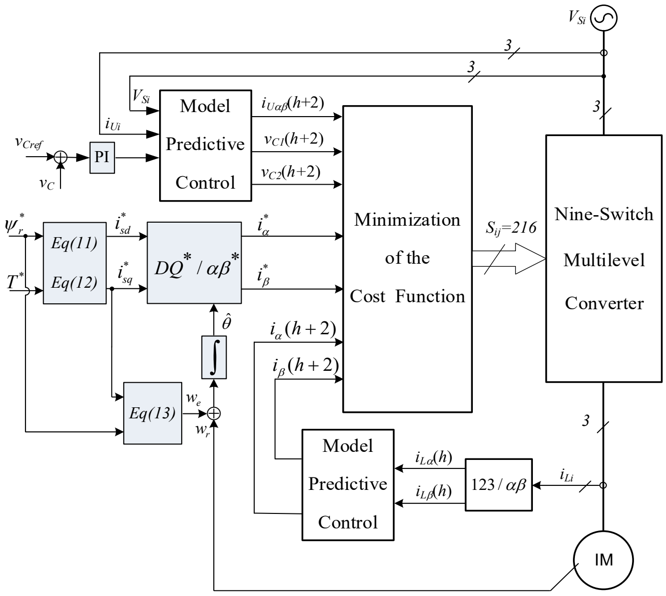

Fig. 2. MPC block diagram for the ANPC-NSMC IM Drive

A. Field Oriented Control

The FOC applied to this motor drive is based on the expressions that describe the induction machine (IM - in squirrel cage), written in a reference frame synchronous with the rotor flux, as shown below [25]:

$$\begin{aligned} \bar{u}_s &= R_s \bar{i}_s + \frac{d\bar{\psi}_s}{dt} + j\omega_r \bar{\psi}_s \\ \bar{u}_r &= R_r \bar{i}_r + \frac{d\bar{\psi}_r}{dt} + j(\omega_r - \omega)\bar{\psi}_r \end{aligned} \tag{8}$$

$$\begin{aligned} \bar{\psi}_s &= L_s \bar{i}_s + L_m \bar{i}_r \\ \bar{\psi}_r &= L_r \bar{i}_r + L_m \bar{i}_s \end{aligned} \tag{9}$$

$$T = -\frac{3}{2} p \bar{i}_r . j\bar{\psi}_r \tag{10}$$

where $\bar{u}_s$ and $\bar{u}_r$ are, respectively, the stator and rotor voltage; $\bar{\psi}_s$ and $\bar{\psi}_r$ the stator and rotor flux, respectively; $\bar{i}_s$ and $\bar{i}_r$ the stator and rotor currents, respectively; L_s, L_r and L_m denotes the stator, rotor and mutual inductances; R_s, R_r are the stator and rotor resistances; ω_r is the angular speed of the rotor flux vector; ω is the rotor angular speed in electric radians and p the number of pole pair.

The FOC principle is widely used in the control of induction machines [25]. This control technique uses of a suitable coordinate system that enables the control of both torque, T, and the rotor flux, ψ_r, independently of each other. Thus, the rotor flux is synchronously oriented to the rotating reference frame. The rotor flux is controlled by the real part of the stator current, i_{sd} while the torque by the imaginary part, Based on these criteria, equations (11) and (12) are the stator currents reference components, i_{sd}^* and i_{sq}^*, that are function respectively of the rotor flux (ψ_r^*) and torque (T^*) references:

$$i_{sd}^* = \frac{\psi_r^*}{L_m} \tag{11}$$

$$i_{sq}^* = \frac{L_r}{L_m}\frac{T^*}{\psi_r^*} \tag{12}$$

The precise determination of the rotor flux vector position angle (θ) for the field orientation, to be used in the Park transformation of the stator current references, is one of the crucial components of the FOC method. This flux angle can be obtained by speed integration, resulting from the addition of rotor speed (ω_r) with the estimator velocity, ω_e, in (13).

$$\omega_e = \frac{L_m}{\tau_r}\frac{i_{sq}^*}{\psi_r^*} \tag{13}$$

Applying the inverse Park transformation (14), to the stator currents references components (i_{sd}^* and i_{sq}^*), $\alpha\beta$ coordinates current references ($i_{s\alpha}^*$ and $i_{s\beta}^*$) are obtained.

$$\begin{bmatrix} i_{s\alpha}^* \\ i_{s\beta}^* \end{bmatrix} = \begin{bmatrix} \cos\theta & -\sin\theta \\ \sin\theta & \cos\theta \end{bmatrix} \begin{bmatrix} i_{sd}^* \\ i_{sq}^* \end{bmatrix} \tag{14}$$

The previously obtained expressions were implemented through Simulink blocks as seen in Fig. 2.

B. Predictive Controller of the Inverter and Rectifier

The controller applied to the IM requires the control of the stator currents. For clarity, from the block diagram of Fig. 2, we will consider the stator induction reference currents ($i_{s\alpha}^*$ and $i_{s\beta}^*$) represented by $i_{L\alpha}^*$ and $i_{L\beta}^*$. Therefore, a MPC is used in the inverter side of the ANPC-NSMC to enforce the α, β components of the stator currents toward their references, $i_{L\alpha}^*$ and $i_{L\beta}^*$ (Fig. 2). To obtain nearly sinusoidal stator currents with smallest current error an appropriate cost functional (g_L) is needed. The main purpose of the optimal predictive controller must be to guarantee the minimum error between the reference current and its predicted value of the stator currents. The proposed cost functional uses the absolute value of the current error [22] taken in the next sampling time (h+2) interval, considering the computational time (h), applied to the stator currents (15) estimated for (h+1).

$$g_L = \left|i_{L\alpha}^*(h+2) - i_{L\alpha}(h+2)\right| + \left|i_{L\beta}^*(h+2) - i_{L\beta}(h+2)\right| \tag{15}$$

where $i_{L\alpha}^*(h+2)$, $i_{L\beta}^*(h+2)$ and $i_{L\alpha}(h+2)$, $i_{L\beta}(h+2)$ are the real and imaginary parts of the stator currents references and the stator currents predicted, two steps forward for the compensation of the computational time spent on the evaluation control algorithm [19]. From the previous criteria and the control scheme in Fig. 2, the stator currents at the t_{h+1} instant, can be predicted according the discrete-time way (16).

$$i_{Li}(h+1)=\left(1-\frac{R_s}{L_s}T_S\right)i_{Li}(h)+\frac{T_S}{L_s}v(h) \quad (16)$$

where $i_{Li}(h)$ is the AC load currents measured and $i_{Li}(h+1)$ is the AC currents to be predicted for the next (h+1) sampling interval, T_S is the sampling time.

Consequently, these stator future currents are acquired by time-shifting the model (17) one step forward as:

$$i_{Li}(h+2)=\left(1-\frac{R_s}{L_s}T_S\right)i_{Li}(h+1)+\frac{T_S}{L_s}v(h+1) \quad (17)$$

The purpose of controlling the rectifier on the grid-connected side is to regulate the DC bus voltage by keeping the sinusoidal input currents in phase with their respective supply line voltages. This is achieved based on predictive control theory applied to the inverter side of the ANPC-NSMC, to minimize a suitable cost function, g_U, as shown in (18).

$$g_U=\left|i_{U\alpha}^*(h+2)-i_{U\alpha}(h+2)\right|+\left|i_{U\beta}^*(h+2)-i_{U\beta}(h+2)\right| \quad (18)$$

From the previous considerations and the control scheme shown in Fig. 2, the grid currents at the t_{h+1} instant, can be predicted according the discrete-time approach (19).

$$i_{Ui}(h+1)=\left(1-\frac{R_g}{L_g}T_S\right)i_{Ui}(h)+\frac{T_S}{L_r}\left(V_{Si}(h)-v(h)\right) \quad (19)$$

where $V_{Si}(h)$ is the grid voltage; $i_{Ui}(h)$ is the AC load currents measured and $i_{Ui}(h+1)$ is the AC currents to be predicted for the next (h+1) sampling interval, T_S is the sampling time.

Consequently, the stator future currents at time (h+2) are computed by time-shifting the model (19) one step forward as:

$$i_{Ui}(h+2)=\left(1-\frac{R_g}{L_g}T_S\right)i_{Ui}(h+1)+\frac{T_S}{L_g}v(h+1) \quad (20)$$

Similarly, the cost function of the DC capacitors voltages imbalance can be defined as:

$$g_{vc}=\left|v_{C1}(h+2)-v_{C2}(h+2)\right| \quad (21)$$

where $v_{C1}(h+2), v_{C2}(h+2)$ are the predicted voltages of the C_1 an C_2, capacitors.

The discrete time equations for the capacitors (C_1 and C_2) voltages, using the MPC theory, are obtained according (22).

$$v_{Ck}(h+1)=v_{Ck}(h)+\frac{1}{C_k}i_{Ck}(h)T_S \quad (22)$$

where the currents $i_{Ck}(h)$ (k=1,2) depend on the switching states of the dual output ANPC-Type inverter and the value of the AC output currents, according to expression (23) and (24):

$$\begin{aligned}i_{C1}(h)=-\big[&d_{A1}i_{UA}+d_{B6}i_{UB}+d_{C11}i_{UC}+\\&d_{A1}d_{A2}i_{LA}+d_{B6}d_{B7}i_{LB}+d_{C11}d_{C12}i_{LC}\big]\end{aligned} \quad (23)$$

$$\begin{aligned}i_{C2}(h)=\big[&d_{A3}i_{LA}+d_{B8}i_{LB}+d_{C13}i_{LC}+\\&d_{A2}d_{A3}i_{UA}+d_{B8}d_{B7}i_{UB}+d_{C13}d_{C12}i_{UC}\big]\end{aligned} \quad (24)$$

where $i_U(h)$, $i_L(h)$ are the currents in the upper and lower sides of the converter DC buses, respectively.

Employing the computational time compensation technique, for the capacitors voltages in (22), the future of the capacitors voltages at the instant (h+2) is obtained as follows:

$$v_{Ck}(h+2)=v_{Ck}(h+1)+\frac{1}{C_k}i_{Ck}(h+1)T_S \quad (25)$$

The proposed cost functional for the dual output three-level inverter MPC control, is given as:

$$g=g_U\rho_U+g_L\rho_L+g_{vc}\rho_{vc} \quad (26)$$

where ρ_U, ρ_L and ρ_{vc} are the weighting factors for the grid currents, for the stator currents and for the imbalance capacitor voltages cost function, respectively.

IV. Simulation Results

Several simulation tests were conducted to test the performance of the grid-tied AC inverter, with a nine-switch multilevel topology feeding an induction machine. The simulation of this power system was implemented in the program *Matlab/Simulink*, using the *SimPowerSystems* library. The Simulink model includes the semiconductor switching behaviour, losses, and all the dynamic behaviour of the induction motor and multilevel converter, as shown in the following results. The following experiments were performed using an induction machine, whose parameters are listed in Table 1 (from the manufacturer's catalogue).

TABLE I. Parameters of the Indution Motor

Variable	Parameter	Value
Stator resistance	R_s	0.59 Ω
Rotor resistance	R_r	0.63 Ω
Stator inductance	L_s	3.5 mH
Stator inductance	L_r	5.4 mH
Mutual inductance	L_m	3.5 mH
Inertial moment	J	0.05Kgm^{2}s^{-1}
Number of pole pair	p	2

The simulation results were obtained initially in steady-state conditions and then in transient conditions, based in different system requirements. Rectifier side of the ANPC-NSMC is connected to the 400V/50Hz grid and on the DC bus are connected the capacitors C_1 and C_2 each with 1 mF capacitance. Figs. 4 and 5 show the results in steady state, when the torque and rotor flux references are 10 Nm and 0.1Wb, respectively. In Fig. 4 the AC currents on the ANPC-NSMC, respectively in the rectifier and inverter side and in Fig. 5 the AC voltages on the ANPC-NSMC, between phase A and B in the rectifier and inverter side, respectively.

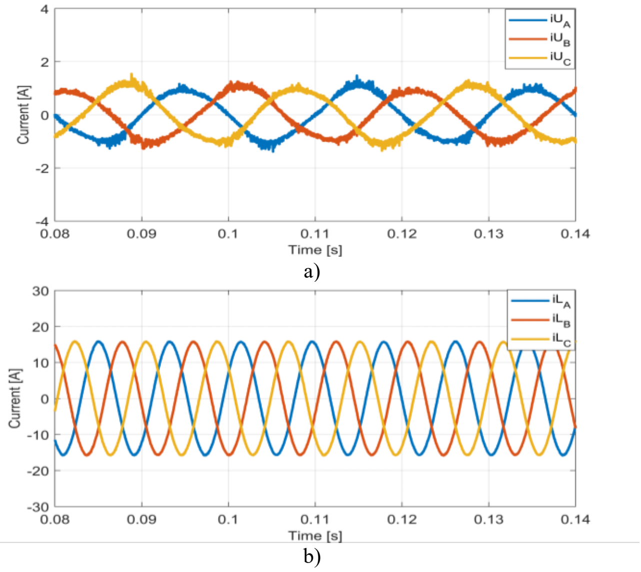

Fig. 3. Waveforms of the AC currents in the nine-switch multilevel converter, in steady-state condition: a) rectifier side; b) inverter side.

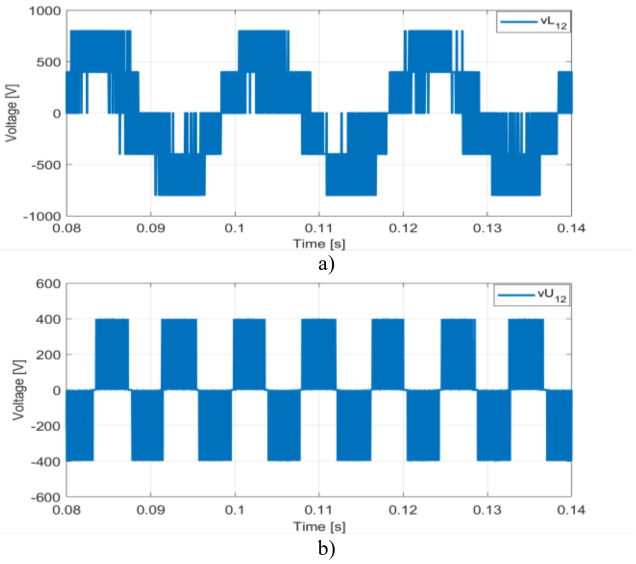

Fig. 4. Waveforms of the AC voltages in the ANPC-NSMC, (between A and B phase) in steady-state condition: a) rectifier side; b) inverter side.

From the results presented in Fig.3 a) it is seen that the AC currents, on the rectifier side, are balanced with relatively small distortion, with a THD equals to 9.86%. The stator currents (in Fig. 3 b)) are also balanced but present much lower distortion than AC currents, with a THD equals to 1.28%. Fig. 4a) shows the 3-level line-to-line voltage, on the rectifier side, while the 5-level line-to-line voltage can be seen in Fig. 4b) on the inverter side, in steady-state conditions. This proves the multilevel operation of this dual output converter. Another significant feature in the proposed control system is the balance of the DC capacitor C_1 and C_2 voltages, which are visible in Fig. 5. This result attests the usefulness of the predictive controller confirming that, apart from the ripple, the voltages V_{C1} and V_{C2} voltage are close to the same value.

The following tests are obtained in dynamic conditions, considering torque reference step transitions. The rotor flux and torque references were initially set 0.2 Wb and 10 Nm, respectively. At instant t=0.3s the torque reference is increased to 25 Nm. Fig. 6 a) shows the rectifier side AC currents balanced and with relatively small distortion. Fig. 6 b), shows the behavior of the three-phase stator currents. When increasing the reference torque the amplitude and the frequency of the stator currents also increase, as expected. For these conditions the stator currents follow the references, obtained from the field orientation control applied to the IM, presenting low distortion, and maintaining balanced currents.

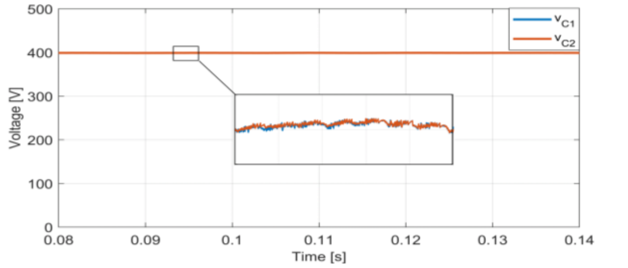

Fig. 5. Result of the capacitors C_1 and C_2 voltages, in steady-state condition.

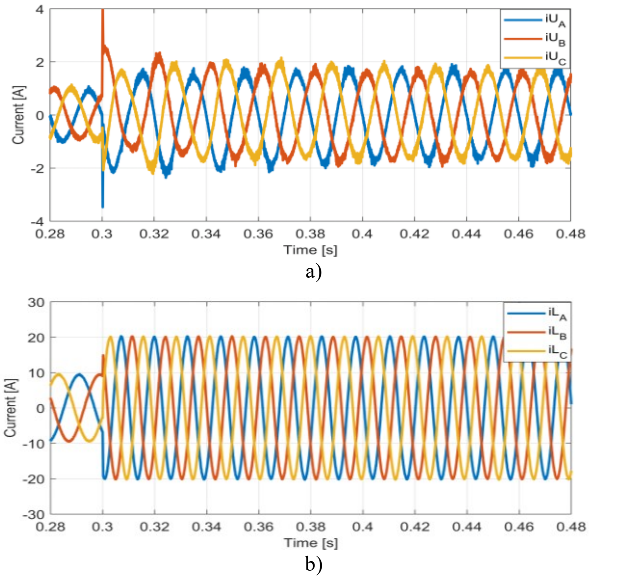

Fig. 6. Waveforms of the AC currents in dynamic conditions, when the rotor flux is 0.2Wb and the torque torque reference is increased to 25 Nm. a) in the rectifier side; b) in the inverter side.

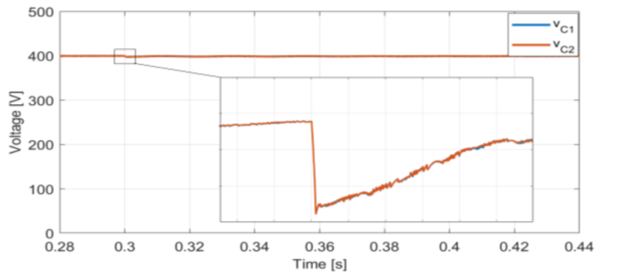

Fig. 7. Results of capacitors C_1 and C_2 voltage in dynamic condition, when the rotor flux is 0.2Wb and the torque torque reference increases to 25 Nm.

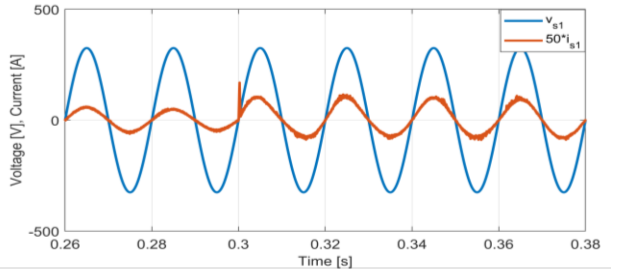

Fig. 8. Results of capacitors C_1 and C_2 voltage in dynamic condition, when the rotor flux is 0.2Wb and the torque torque reference increases to 25 Nm.

The balance of the DC capacitor voltages was also tested in dynamic conditions, when the torque reference is increased to 25 Nm maintaining the rotor flux at 0.2Wb. Fig.7 shows that the capacitor voltages have a small disturbance (leading to higher charging currents) but remain stable and close to the reference values. Fig. 8 presents the current and voltage in phase A of the rectifier side of the multilevel converter. The current waveform 50*I_{s1} shows that the current is in phase with the same phase grid voltage also in transient mode.

V. Conclusions

A back-to-back solution with ANPC-NSMC topology, from a three-level ANPC-type structure inverter, is proposed in this paper. This multilevel converter topology is connected to the grid in the rectifier side and is connected to an induction motor in the inverter side. To control the inverter side of the multilevel, a field-oriented controller was used, together with a current mode predictive control strategy for the IM stator currents. The rectifier side was controlled by a PI controller, to regulate the DC link voltage, aided by a current mode predictive control. The MPC was developed with the purpose of controlling not only the AC currents, of each side of the multilevel converter, but also to maintain the DC capacitor voltages balanced. The control system has been validated through several simulation tests. From the obtained results in steady-state and dynamic conditions, it was seen that the proposed control approach allows good control performances and is suited to this specific multilevel converter topology presenting 216 voltage vectors. As future work, it will be studied the operation of this drive in fault tolerant mode for an open switch fault.

Acknowledgment

This work was supported by national funds through FCT, Fundação para a Ciência e a Tecnologia, under project UIDB/50021/2020 (DOI:10.54499/UIDB/50021/2020).

References

[1] L. G. Franquelo, J. Rodriguez, J. I. Leon, S. Kouro, R. Portillo and M. A. M. Prats, "The age of multilevel converters arrives," in IEEE Industrial Electronics Magazine, vol. 2, no. 2, pp. 28-39, June 2008.

[2] S. Kouro et al.,"Recent Advances and Industrial Applications of Multilevel Converters," in IEEE Transactions on Industrial Electronics, vol. 57, no. 8, pp. 2553-2580, August 2010.

[3] F. Blaabjerg, Y. Yang, K. Ma, X. Wang,"Power electronics - the key technology for renewable energy system integration" Int. Conf. Renewable Energy Research Appl., pp. 1618-1626, Nov. 2015.

[4] A. Nabae, I. Takahashi and H. Akagi, "A new neutral-point-clamped PWM inverter", IEEE Trans. Ind. Appl., vol. IA-17, no. 5, pp. 518-523, Sep./Oct. 1981.

[5] T. A. Meynard and H. Foch, "Multi-level choppers for high voltage applications", EPE Journal, vol. 2, no. 1, pp. 45-50, March 1992.

[6] P. W. Hammond, "A new approach to enhance power quality for medium voltage ac drives", IEEE Trans. Ind. Appl., vol. 33, no. 1, pp. 202-208, Jan./Feb. 1997.

[7] V. F. Pires, A. Cordeiro, D. Foito, J. F. Silva and E. Romero-Cadaval, "Cascaded Multilevel Structure With Three-Phase and Single-Phase H-Bridges for Open-End Winding Induction Motor Drive," IEEE Open Journal of the Industrial Electronics Society, vol. 4, pp. 346-361, August 2023.

[8] M. Schweizer and J. W. Kolar, "Design and Implementation of a Highly Efficient Three-Level T-Type Converter for Low-Voltage Applications", IEEE Trans. on Power Electronics, vol. 28, no. 2, pp. 899-907, Feb. 2013.

[9] M. M. Qasim, D. M. Otten, J. H. Lang, J. L. Kirtley and D. J. Perreault, "Comparison of Inverter Topologies for High-Speed Motor Drive Applications," in IEEE Transactions on Power Electronics, doi: 10.1109/TPEL.2024.3376196.

[10] V. F. Pires, J. Monteiro, J. Fernando Silva and S. Pinto, "A Model Predictive Control for a Multilevel Inverter Fed Induction Motor Drive Based on Three-Phase Triple Inverter Modular Topology" International Symposium on Industrial Electronics and Applications, pp. 1-6, 2022.

[11] S. Debnath, J. Qin, B. Bahrani, M. Saeedifard and P. Barbosa "Operation, Control, and Applications of the Modular Multilevel Converter: A Review" IEEE Trans. on Power Elect., vol.30, no.1, pp.37-53, Jan. 2015.

[12] V. F. Pires, A. Cordeiro, D. Foito and J. F. Silva, "A Multilevel Converter Topology for a STATCOM System Based on Four-Leg Two-Level Inverters and Cascaded Scott Transformers," IEEE Transactions on Power Delivery, vol. 37, no. 3, pp. 1391-1402, June 2022.

[13] S. Arazm and K. Al-Haddad, "A Novel Single DC Source Three-Phase Wye Packed U-Cell (Y-PUC) Converter," in IEEE Open Journal of the Industrial Electronics Society, vol. 3, pp. 1-13, December 2021.

[14] T. Kominami, Y. Fujimoto, "Inverter with Reduced Switching-Device Count for Independent AC Motor Control," Industrial Electronics Society 2007, pp.1559- 1564, 2007.

[15] J. Haruna and N. Hoshi, "A Novel Three-level inverter which can drive two PMSMs," 7th IET International Conference on Power Electronics, Machines and Drives (PEMD 2014), Manchester, UK, 2014, pp. 1-6.

[16] R. Wang, L. Ai and C. Liu, "A Novel Three-Phase Dual-Output Neutral-Point-Clamped Three-Level Inverter," in IEEE Transactions on Power Electronics, vol. 36, no. 7, pp. 7576-7586, July 2021.

[17] C. N. Jibhakate, M. A. Chaudhari and M. M. Renge, "Reactive Power Compensation Using Induction Motor Driven by Nine Switch AC-DC-AC Converter," in IEEE Access, vol. 6, pp. 1312-1320, 2018

[18] S. M. Dabour, A. S. Abdel-Khalik, S. Ahmed and A. Massoud, "An Optimal PWM Technique for Dual-Output Nine-Switch Boost Inverters With Minimum Passive Component Count," IEEE Transactions on Power Electronics, vol. 36, no. 1, pp. 1065-1079, Jan. 2021.

[19] P. R. U. Guazzelli et al., "Decoupled Predictive Current Control With Duty-Cycle Optimization of a Grid-Tied Nine-Switch Converter Applied to an Induction Generator," in IEEE Transactions on Power Electronics, vol. 37, no. 3, pp. 2778-2789, March 2022.

[20] S. Bayhan, M. Trabelsi, H. Abu-Rub, M. Malinowski, "Finite-Control-Set Model-Predictive Control for a Quasi-Z-Source Four-Leg Inverter Under Unbalanced Load Condition," IEEE Transactions on Industrial Electronics, vol. 64, no. 4, pp. 2560–2569, April 2017..

[21] J. Monteiro, V. F. Pires, J. F. Silva and S. Pinto, "Mutilevel Bipolar Back-to-Back HVDC Transmission System Based on the Dual Inverter Converter Structure with Model Predictive Control" IECON22 48th Annual Conference of the IEEE Ind. Elect. Society, pp. 1-6, Oct. 2022.

[22] M. Rivera, V. Yaramasu, A. Llor, J. Rodriguez, B. Wu, M. Fadel, "Digital predictive current control of a three-phase four-leg inverter," IEEE Trans. Ind. Electron., vol. 60, no. 11, pp. 4903–4912, Nov. 2013.

[23] J. Monteiro, V. F. Pires, J. F. Silva and S. Pinto, "A Dual-Output NPC-Type Converter with a Model Predictive Controller with Compensation of DC Capacitor Voltage Imbalance," 17th International Conference on Compatibility, Power Electronics and Power Engineering, pp. 1-6, 2023.

[24] J. D. Barros and J. F. Silva, "Multilevel Optimal Predictive Dynamic Voltage Restorer," in IEEE Transactions on Industrial Electronics, vol. 57, no. 8, pp. 2747-2760, Aug. 2010.

[25] Blaschke, F. The principle of field-orientation as applied to the new transvector closed-loop system for rotating-field machines. Siemens Rev. 1972, 34, 217–220.